Multichannel ultracold collisions between metastable bosonic ^{88}Sr and fermionic ^{87}Sr atoms

Deshui Yu*

Department of Applied Physics, Graduate School of Engineering, The University of Tokyo, Bunkyo-ku, Tokyo 113-8656, Japan and Innovative Space-Time Project, ERATO, Japan Science and Technology Agency, Bunkyo-ku, Tokyo 113-8656, Japan

(Received 20 July 2012; published 6 September 2012)

Ultracold collisions between metastable bosonic ^{88}Sr [$(5s5p)\,^3P_2$] and fermionic ^{87}Sr [$(5s5p)\,^3P_2$ ($i = 9/2$)] atoms are investigated based on an approach of tensorial analysis. The scattering physics of two atoms in fully polarized s-wave entrance channels is studied in detail. In the Born-Oppenheimer approximation, the strong anisotropic interatomic interaction is demonstrated to induce formations of long-range molecular potential wells. However, besides significantly modifying the elastic scattering, the anisotropic interatomic interaction leads to the strong multichannel coupling between different partial waves, which triggers a high rate of inelastic losses. By applying an external static magnetic field $\mathbf{B}_0 = \mathcal{B}_0\mathbf{e}_z$, the inelastic scattering can be suppressed while the elastic scattering is significantly enhanced. Additionally, the energy-dependent complex s-wave scattering lengths at a given relative collision energy strongly depend on the strength of magnetic field. We, moreover, self-consistently investigate ultracold collisions of two atoms at low temperatures in an optical lattice site. In the δ-function pseudopotential approximation, we derive the effective s-wave scattering lengths, energy eigenvalues, elastic and inelastic scattering rates, and their dependence on the external magnetic field. We find that (i) the effective scattering lengths of ultracold atoms in entrance channels of interest display resonance behavior at certain values of magnetic field and (ii) the extra Zeeman interaction not only leads to the suppression of inelastic scattering but also enlarges the elastic scattering rates.

DOI: 10.1103/PhysRevA.86.032703 PACS number(s): 34.20.Cf, 34.50.Cx

I. INTRODUCTION

Recently, alkaline-earth-metal atoms have moved into the focus of interest in atomic physics and offered many possibilities for practical application and fundamental studies; e.g., an optical Ramsey-Bordé atomic interferometer based on ^{40}Ca [1] is a powerful tool for precise frequency and phase measurements in modern science, an optical lattice clock [2–4] with a large number of ultracold strontium atoms separately trapped in the Lamb-Dicke regimes and with a zero net ac Stark shift of the clock $(5s^2)\,^1S_0$-$(5s5p)\,^3P_0$ transition is being developed toward the realization of the next-generation atomic clock, a complete scheme for quantum information processing can be realized, in principle, based on ^{87}Sr [5], omnidirectional photonic band gaps have been theoretically proved in dipolar atomic lattices formed by the ultracold ^{88}Sr atoms [6,7], etc. All of these applications are based on the unique features of alkaline-earth-metal atoms, which have a spin-nondegenerate electronic ground $(ns^2)\,^1S_0$ state and can be easily cooled down to a Doppler temperature of the order of mK by using the strong dipole $(ns^2)\,^1S_0$-$(nsnp)\,^1P_1$ transition. Due to two valence electrons, alkaline-earth-metal atoms display spin singlet- and triplet-level manifolds at low excitation energies, which give rise to narrow intercombination $(ns^2)\,^1S_0$-$(nsnp)\,^3P_1$ transitions. By exploiting this transition line, Katori *et al.* [8] achieved a ^{88}Sr atomic gas at a temperature of 1 μK, and Binnewies *et al.* [9] cooled a cloud of ^{40}Ca atoms down to 10 μK. Recently, Bose-Einstein condensations of ^{84}Sr [10,11], ^{86}Sr [12], and ^{40}Ca [13] have been realized via the last evaporating cooling stage.

Alkaline-earth-metal atoms in their lowest metastable $(nsnp)\,^3P_2$ level are exceptionally long-lived [14] and can be magnetically trapped [15]. Due to the nonzero angular momenta, the nonspherical atomic structure leads to anisotropic long-range interactions between two metastable alkaline-earth-metal atoms. This anisotropy affects the rotational motion of the diatomic system and couples states of different rotational quantum numbers. Based on a diatomic system of practical interest, i.e., two ^{88}Sr atoms in the metastable $(5s5p)\,^3P_2$ excited state, Derevianko *et al.* [16] were the first to theoretically approach the problem of anisotropic long-range interactions between metastable alkaline-earth-metal atoms in an external magnetic field and predicted the existence of a long-range molecular potential well for the electronic state of the highest Zeeman energy. Almost at the same time, Santra and Greene [17] studied the same system via an approach of tensorial analysis and gave a similar qualitative prediction. The scattering length on this potential well can be tuned by adjusting the magnetic-field strength, which enables the control of sign and strength of the effective interatomic interaction at ultracold temperatures. Additionally, Kokoouline *et al.* [18] pointed out that the strong coupling between different partial waves of relative motion not only modifies the shape of adiabatic potential-energy curves but also produces larger nonadiabatic dynamical effects, hence the large inelastic losses.

So far, most realistic theoretical treatments of ultracold collisions and the corresponding experiments have ignored the effect of hyperfine coupling on the short-range interatomic interaction because of the relatively smaller energy of the hyperfine-structure splitting. However, the hyperfine interaction plays an important role in the ultracold collision dynamics, especially the collision loss induced by the hyperfine coupling [19]. Additionally, the large number of hyperfine and magnetic sublevel combinations can give rise to numerous individual interatomic potentials and the possibility of the existence of

*dsyu@amo.t.u-tokyo.ac.jp

long-range molecular potential wells because of the numerous avoided crossings [20].

In this paper, we investigate ultracold collisions between bosonic ^{88}Sr and fermionic ^{87}Sr atoms in their metastable $(5s5p)\,^3P_2$ state with the hyperfine interaction of ^{87}Sr being taken into account. For two atoms in fully polarized s-wave entrance channels, all collision dynamics at ultracold temperatures ($<10\,\mu$K) take place at interatomic distances of about 10^2 Bohr radii, which justifies a pure long-range description. In the adiabatic (Born-Oppenheimer) approximation, the s-wave entrance channels of interest have long-range molecular potential wells arising due to the avoided crossings. However, since the anisotropic interatomic interaction leads to the pronounced coupling between different partial waves of relative motion, the strong multichannel coupling causes large inelastic losses in addition to significantly modifying the elastic scattering. Nevertheless, based on the coupled multichannel-scattering calculation, we find that by applying an external magnetic field the extra Zeeman interaction not only can suppress the inelastic scattering but also can enhance the elastic scattering of ultracold atoms in entrance channels of interest. Finally, we investigate ultracold collisions of two atoms confined in an optical lattice site. The effective s-wave scattering lengths, elastic and inelastic scattering rates, and their dependence on the external magnetic field are self-consistently computed via the coupled multichannel-scattering calculation.

This paper is organized as follows. In Sec. II we provide a systematic framework for describing anisotropic interatomic interactions based on an approach of tensorial analysis, where we take into account the long-range electric dipole-dipole, quadrupole-quadrupole, and dipole-quadrupole interactions as well as the magnetic dipole-dipole interaction. In Sec. III, we numerically diagonalize the Hamiltonian matrix of interatomic interactions so as to derive the adiabatic potential-energy curves. The elastic and inelastic scattering rates and the energy-dependent s-wave scattering lengths of atoms in fully polarized s-wave entrance channels are computed via the coupled multichannel-scattering calculation. Ultracold collisions at low temperatures in the presence of an external magnetic field are considered in Sec. IV. Section V is devoted to investigating the scattering physics of two atoms confined in an optical lattice site. We first study how to realize a three-dimensional isotropic optical lattice. Then, in the δ-function pseudopotential approximation, we self-consistently calculate the effective s-wave scattering lengths, energy eigenvalues, elastic and inelastic collision rates, and their dependence on the external magnetic field. Finally, we summarize our discussion in Sec. VI.

II. HAMILTONIAN OF COLLISION BETWEEN TWO ATOMS

The complete Hamiltonian describing the relative (rel) motion of two interacting atoms, a (^{88}Sr) and b (^{87}Sr), can be written as

$$H_{\rm rel} = -\frac{\hbar^2}{2m}\left(\frac{\partial^2}{\partial r^2}+\frac{2}{r}\frac{\partial}{\partial r}\right)+\frac{\mathbf{L}^2}{2mr^2}+V_{\rm int}(r)+H_{\rm hpf}(b), \tag{1}$$

where $m = m_a m_b/(m_a+m_b)$ is the reduced mass with $m_{a,b}$ masses of atoms ^{88}Sr and ^{87}Sr, $r = |\mathbf{r}_a - \mathbf{r}_b|$ is the internuclear distance, $\mathbf{r}_a$ and $\mathbf{r}_b$ are absolute positions of two nuclei in the *space-fixed* frame, $\mathbf{L}$ is the angular momentum associated with the rotation of the molecular frame, and $V_{\rm int}(r)$ is the interatomic interaction including the electric dipole-dipole ($\sim r^{-3}$), quadrupole-quadrupole ($\sim r^{-5}$), dipole-quadrupole ($\sim r^{-4}$), and magnetic dipole-dipole ($\sim r^{-3}$) interactions. $H_{\rm hpf}(b)$ describes the hyperfine interaction of fermionic ^{87}Sr. For a diatomic system, the wave function for a bound or scattering state of the relative motion can be described in a close-coupling expansion as $\psi_\alpha(E,\mathbf{r}) = \sum_\alpha \frac{\phi_{\alpha',\alpha}(E,r)}{r}|\alpha'(\mathbf{r})\rangle$, where E is the total energy of internal states and relative motion of two atoms. The expansion basis $\{|\alpha(\mathbf{r})\rangle\}$ is an implicit function of $\mathbf{r}$, which equals the asymptotic channel state basis as $r\to\infty$.

For two atoms, ^{88}Sr and ^{87}Sr, at long-range interatomic distance $r > 50$ Bohr radii, two electron clouds do not overlap each other, and atoms can be identified by their respective nuclei. Thus, the splitting between neighboring atomic energy levels corresponding to the same fine-structure manifold of a single atom is much larger than energies of interatomic interactions. Consequently, both atoms are in the same well-defined fine-structure level $(5s5p)\,^3P_2$.

Without the interatomic coupling, the full Hilbert space of the diatomic system in the *body-fixed* frame is spanned by the direct products of single-atom states $|\xi,j,m_j\rangle_a|\xi,j,i,f,m_f\rangle_b$. $j=2$ is the electron's total angular momentum quantum number of the LS coupling for both ^{88}Sr and ^{87}Sr with a projection of m_j on the body-fixed axis. $i_b = 9/2$ denotes the nuclear spin of ^{87}Sr. f_b represents the total angular momentum of ^{87}Sr resulting from the magnetic interaction between momenta of j_b and i_b. The projection of f_b on the body-fixed axis is m_f. ξ symbolizes all other electronic quantum numbers of a single atom. For two-body collision, an individual fragmentation channel to the dissociation limit ($r\to\infty$) can be specified by $|(\xi,j)_a,(\xi,j,i,f)_b,F,M_F\rangle$, where the angular moment F results from the coupling between j_a and f_b and M_F is the corresponding projection on the internuclear axis.

A. Interatomic interactions in the body-fixed frame

We follow the approach of tensorial analysis developed in Ref. [17] to consider the expression of the interatomic interaction $V_{\rm int}(r)$, which arises from the multipole interactions between two atoms, in the body-fixed frame. The electrostatic multipole moments of an electron cloud can be written as spherical tensors $\mathbf{q}^{(l)}$ with components [21]

$$q_{l,m} = -\sum_{u=1}^{N} e r_u^l \mathcal{G}_{l,m}(\theta_u,\varphi_u), \tag{2}$$

where e is the electron's charge, u denotes the uth electron with the spherical coordinates (r_u,θ_u,φ_u), and $m=-l,\ldots,l$.

$$\mathcal{G}_{l,m}(\theta,\varphi) = \sqrt{\frac{4\pi}{2l+1}}Y_{l,m}(\theta,\varphi) \tag{3}$$

is a Racah spherical harmonic with $Y_{l,m}(\theta,\varphi)$ being the spherical harmonic function. For two atoms, a and b, the interaction between multipoles $\mathbf{q}^{(l_a)}$ and $\mathbf{q}^{(l_b)}$ can be expressed

in the well-known spherical expansion

$$V(\mathbf{q}^{(l_a)},\mathbf{q}^{(l_b)},\mathbf{r}) = \sum_{m_a}\sum_{m_b} c_{l_a,l_b,m_a,m_b}\frac{q_{l_a,m_a}q_{l_b,m_b}}{r^{l_a+l_b+1}}\mathcal{G}_{l_a+l_b,-m_a-m_b}(\theta,\varphi), \quad (4)$$

where $m_{a,b} = -l_{a,b},\ldots,l_{a,b}$ and c_{l_a,l_b,m_a,m_b} is defined as

$$c_{l_a,l_b,m_a,m_b} = (-1)^{l_b}\sqrt{\frac{(2l_a+2l_b+1)!}{(2l_a)!(2l_b)!}}\begin{pmatrix} l_a & l_b & l_a+l_b \\ m_a & m_b & -m_a-m_b\end{pmatrix}. \quad (5)$$

One can see that $V(\mathbf{q}^{(l_a)},\mathbf{q}^{(l_b)},\mathbf{r})$ only depends on the relative internuclear coordinate r rather than the absolute coordinate $\mathbf{r}_{a,b}$ of each atom. In the body-fixed frame, the z axis is chosen to be along the internuclear axis. Thus, the electric dipole-dipole $V_{dd} \equiv V(\mathbf{q}^{(1_a)},\mathbf{q}^{(1_b)},\mathbf{r})$, quadrupole-quadrupole $V_{qq} \equiv V(\mathbf{q}^{(2_a)},\mathbf{q}^{(2_b)},\mathbf{r})$, and dipole-quadrupole $V_{dq} \equiv V(\mathbf{q}^{(1_a)},\mathbf{q}^{(2_b)},\mathbf{r}) + V(\mathbf{q}^{(2_a)},\mathbf{q}^{(1_b)},\mathbf{r})$ interactions can be written as [17]

$$V_{dd} = -\frac{1}{r^3}\left(q_{1_a,1_a}q_{1_b,-1_b} + 2q_{1_a,0_a}q_{1_b,0_b} + q_{1_a,-1_a}q_{1_b,1_b}\right), \quad (6)$$

$$V_{qq} = \frac{1}{r^5}\left(q_{2_a,2_a}q_{2_b,-2_b} + 4q_{2_a,1_a}q_{2_b,-1_b} + 6q_{2_a,0_a}q_{2_b,0_b} + 4q_{2_a,-1_a}q_{2_b,1_b} + 4q_{2_a,-2_a}q_{2_b,2_b}\right), \quad (7)$$

$$V_{dq} = -\frac{\sqrt{3}}{r^4}\left(q_{1_a,1_a}q_{2_b,-1_b} + \sqrt{3}q_{1_a,0_a}q_{2_b,0_b} + q_{1_a,-1_a}q_{2_b,1_b} - q_{2_a,1_a}q_{1_b,-1_b} - \sqrt{3}q_{2_a,0_a}q_{1_b,0_b} - q_{2_a,-1_a}q_{1_b,1_b}\right), \quad (8)$$

and, similarly, the magnetic dipole-dipole interaction $V_{\mu\mu} \equiv V(\boldsymbol{\mu}^{(1_a)},\boldsymbol{\mu}^{(1_b)},\mathbf{r})$ reads

$$V_{\mu\mu} = -\frac{1}{r^3}\left(\mu_{1_a,1_a}\mu_{1_b,-1_b} + 2\mu_{1_a,0_a}\mu_{1_b,0_b} + \mu_{1_a,-1_a}\mu_{1_b,1_b}\right). \quad (9)$$

Here we have chosen atomic units in the above expressions; i.e., the length is in units of the Bohr radius $a_0 \approx 0.053$ nm, and the energy is in units of rydbergs (13.6 eV). The magnetic dipole tensors of two atoms are defined as

$$\boldsymbol{\mu}^{(1_a)} = -\mu_B\left(g_l\mathbf{l}^{(1_a)} + g_s\mathbf{s}^{(1_a)}\right), \quad (10)$$

$$\boldsymbol{\mu}^{(1_b)} = -\mu_B\left(g_l\mathbf{l}^{(1_b)} + g_s\mathbf{s}^{(1_b)} + g_i\mathbf{i}^{(1_b)}\right), \quad (11)$$

where μ_B is the Bohr magneton, $\mathbf{l}^{(1_{a,b})}$ is the orbital angular momentum of an atom, $\mathbf{s}^{(1_{a,b})}$ is the spin angular momentum, and the electronic Landé g factors are $g_l = 1$ and $g_s = 2.002319$. The Landé g factor for the nuclear spin $\mathbf{i}^{(1_b)}$ of ^{87}Sr is $g_i = -0.000131753$ [22,23]. By using definitions of tensors

$$\mathbf{D}^{(L)} = \left[\mathbf{q}^{(1_a)} \otimes \mathbf{q}^{(1_b)}\right]^{(L)}, \quad (12)$$

$$\mathbf{Q}^{(L)} = \left[\mathbf{q}^{(2_a)} \otimes \mathbf{q}^{(2_b)}\right]^{(L)}, \quad (13)$$

$$\mathbf{M}^{(L)} = \left[\boldsymbol{\mu}^{(1_a)} \otimes \boldsymbol{\mu}^{(1_b)}\right]^{(L)}, \quad (14)$$

all multipole interactions can be simplified as

$$V_{dd} = -\frac{\sqrt{6}}{r^3}D_{2,0}, \quad (15)$$

$$V_{qq} = \frac{\sqrt{70}}{r^5}Q_{4,0}, \quad (16)$$

$$V_{\mu\mu} = -\frac{\sqrt{6}}{r^3}M_{2,0}. \quad (17)$$

The zero components of second-rank tensors $\mathbf{D}^{(2)}$ and $\mathbf{M}^{(2)}$ are related to electric and magnetic dipole-dipole interaction operators V_{dd} and $V_{\mu\mu}$, respectively. V_{qq} depends on the zero component of a fourth-rank tensor $\mathbf{Q}^{(4)}$.

In the electronic fine-structure Hilbert space of the diatomic system, the basis of degenerate model space in the coupled representation reads $\{|(\xi,j)_a,(\xi,j)_b,J,M_J\rangle\}$, where J is the total electronic angular momentum of the $(\xi,j)_a$ and $(\xi,j)_b$ coupling and M_J is the projection of J on the internuclear axis. In this model space, we conclude that

$$\langle(\xi,j)_a,(\xi,j)_b,J,M_J|V_{dd}|(\xi,j)_a,(\xi,j)_b,J',M_J'\rangle = 0 \quad (18)$$

and

$$\langle(\xi,j)_a,(\xi,j)_b,J,M_J|V_{dq}|(\xi,j)_a,(\xi,j)_b,J',M_J'\rangle = 0 \quad (19)$$

because all atomic eigenstates comprising the model space have the same parity. Thus, we need to consider the perturbation induced by the coupling of electronic states inside the model space to those outside the model space via the dispersion interactions of V_{dd} and V_{dq}. The atomic eigenstates in the coupled representation can be expanded by eigenstates $\{|(\xi,j)_a,(\xi,j)_b\rangle \equiv |(\xi,j)\rangle_a|(\xi,j)\rangle_b\}$ in the uncoupled representation via Clebsch-Gordan coefficients.

To the second-order perturbation, the Hamiltonian of the interatomic interaction can be written as

$$V_{\rm int}(r) = \mathscr{P}(V_{\mu\mu} + V_{qq} + V_{\rm dis})\mathscr{P}, \quad (20)$$

where the projection operator is

$$\mathscr{P} = \sum_{J,M_J}|(\xi,j)_a,(\xi,j)_b,J,M_J\rangle\langle(\xi,j)_a,(\xi,j)_b,J,M_J| \quad (21)$$

of the model space,

$$V_{\rm dis} = V_{dd}\mathscr{O}\{E_0[(\xi,j)_a,(\xi,j)_b] - \mathscr{O}H_0\mathscr{O}\}^{-1}\mathscr{O}V_{dd} \quad (22)$$

is the Hamiltonian of the electric dipole-dipole dispersion interaction, H_0 is the Hamiltonian of the noninteracting system with corresponding energy eigenvalues

$$E_0[(\xi,j)_a,(\xi,j)_b] = \langle(\xi,j)_a,(\xi,j)_b|H_0|(\xi,j)_a,(\xi,j)_b\rangle, \quad (23)$$

and $\mathscr{O} = 1 - \mathscr{P}$. Here we have neglected the perturbation of electric dipole-quadrupole interaction V_{dq}, which is proportional to r^{-8} and mainly affects the short-range interaction potential of the relative motion. Following the same approach in Ref. [17], we can prove that the interatomic Hamiltonian $V_{\rm int}(r)$ is related to the reduced matrix elements $M(f,f',F,F') \equiv \langle\beta||\mathbf{M}^{(2)}||\beta'\rangle$, $Q(f,f',F,F') \equiv \langle\beta||\mathbf{Q}^{(2)}||\beta'\rangle$, $I_K(f,f',F,F') \equiv \langle\beta||\mathbf{I}^{(K)}||\beta'\rangle$, $(|\beta\rangle = |(\xi,j)_a,(\xi,j,i,f)_b,F\rangle$, and $|\beta'\rangle = |(\xi,j)_a,(\xi,j,i,f')_b,F'\rangle)$,

i.e.,

$$M(f,f',F,F',i) = \frac{\sqrt{30}}{2} g_{ls} \sqrt{[f,F,2,f',F']} \begin{Bmatrix} 2 & 2 & 1 \\ f & f' & 1 \\ F & F' & 2 \end{Bmatrix} \times \left[(-1)^{i+f'} \frac{\sqrt{30}}{2} \begin{Bmatrix} f & 1 & f' \\ 2 & i & 2 \end{Bmatrix} g_{ls} + (-1)^{i+f} \sqrt{i(i+1)} \begin{Bmatrix} f & 1 & f' \\ i & 2 & i \end{Bmatrix} g_i \right] \mu_B^2, \tag{24}$$

$$Q(f,f',F,F',i) = (-1)^{i+f'} \sqrt{[f,F,4,f',F']} \begin{Bmatrix} 2 & 2 & 2 \\ f & f' & 2 \\ F & F' & 4 \end{Bmatrix} \begin{Bmatrix} f & 2 & f' \\ 2 & i & 2 \end{Bmatrix} \langle q_2 \rangle^2, \tag{25}$$

$$I_K(f,f',F,F',i) = \sum_{J=|j-f|}^{j+f} \sum_{J'=|j-f'|}^{j+f'} (-1)^{F+i+J'} \frac{[J,2,J']}{3} \sqrt{[f,F,K,f'F']} \begin{Bmatrix} 2 & 2 & J \\ i & F & f \end{Bmatrix} \begin{Bmatrix} 2 & 2 & J' \\ i & F' & f' \end{Bmatrix} \begin{Bmatrix} F & K & F' \\ J' & i & J \end{Bmatrix} \mathcal{W}_{K,J,J'}, \tag{26}$$

where $g_{ls} \equiv g_l + g_s$, $[n] = 2n+1$, and $K = 0,2,4$. $\langle q_2 \rangle \equiv \langle (5s5p)\,^3P_2 || \mathbf{q}^{(2)} || (5s5p)\,^3P_2 \rangle \approx 34.3$ a.u. denotes the electric quadrupole moment of the atomic $(5s5p)\,^3P_2$ state [24], and the function $\mathcal{W}_{K,J,J'}$ is defined as

$$\mathcal{W}_{K,J,J'} = \sum_{j_1,j_2} \tilde{C}_6^{j_1,j_2} \sum_{\tilde{J}=|j_1-j_2|}^{j_1+j_2} [\tilde{J}] \begin{Bmatrix} 2 & 2 & K \\ J & J' & \tilde{J} \end{Bmatrix} \begin{Bmatrix} 2 & j_1 & 1 \\ 2 & j_2 & 1 \\ J & \tilde{J} & 2 \end{Bmatrix} \begin{Bmatrix} j_1 & 2 & 1 \\ j_2 & 2 & 1 \\ \tilde{J} & J' & 2 \end{Bmatrix}. \tag{27}$$

$j_{1,2}$ denote the total angular momenta of any other fine-structure levels outside the model space. The intermediate (uncoupled) dispersion coefficients $\tilde{C}_6^{j_1,j_2}$ have been listed in Ref. [16]. Here we should note that Eqs. (24)–(26) are also suitable for other alkaline-earth-metal atoms, such as ultracold collisions between bosonic ^{24}Mg $[(3s3p)\,^3P_2]$ and fermionic ^{25}Mg $[(3s3p)\,^3P_2$ $(i = \frac{5}{2})]$ atoms and ultracold collisions between bosonic ^{40}Ca $[(4s4p)\,^3P_2]$ and fermionic ^{43}Ca $[(4s4p)\,^3P_2 (i = \frac{7}{2})]$ atoms.

B. Hamiltonian in the space-fixed frame

Above we have only considered interatomic interactions in the body-fixed frame; i.e., the diatomic axis is chosen as the quantization direction. However, the relative movement of the diatomic axis to the *laboratory-fixed* quantization axis leads to a coupling between molecular rotations and electronic degrees of freedom. We need to transform the expression of $V_{\rm int}(r)$ from the body-fixed space to the space-fixed frame, for which we choose the asymptotic fragmentation channel basis $\{|\alpha(\mathbf{r})\rangle\}$ in the laboratory frame as $\{|l,(\xi,j)_a,(\xi,j,i,f)_b,F,T,M_T\rangle\}$, where l is the angular momentum quantum number associated with the rotation of the molecular frame, T is the total angular moment resulting from the coupling between l and F, and M_T is the projection of T on the space-fixed axis. Following the same approach in Ref. [17], we obtain the matrix element of the interatomic interaction $V_{\rm int}$ between collision channels $|\alpha\rangle \equiv |\alpha(r \to \infty)\rangle = |l,(\xi,j)_a,(\xi,j,i,f)_b,F,T,M_T\rangle$ and $|\alpha'\rangle \equiv |\alpha'(r \to \infty)\rangle = |l',(\xi,j)_a,(\xi,j,i,f')_b,F',T',M_T'\rangle$,

$$\langle \alpha | V_{\rm int}(r) | \alpha' \rangle = \delta_{T,T'} \delta_{M_T,M_T'} \sum_{n=3,5,6} \frac{F_n(l,l',f,f',F,F',T)}{r^n}, \tag{28}$$

where the r^{-n}-dependent parameters read

$$F_3(l,l',f,f',F,F',T,i) = (-1)^{F+T+1} \sqrt{[l,l']} \sqrt{6} \begin{pmatrix} l' & 2 & l \\ 0 & 0 & 0 \end{pmatrix} \begin{Bmatrix} l & F & T \\ F' & l' & 2 \end{Bmatrix} M(f,f',F,F',i), \tag{29}$$

$$F_5(l,l',f,f',F,F',T,i) = (-1)^{F+T} \sqrt{[l,l']} \sqrt{70} \begin{pmatrix} l' & 4 & l \\ 0 & 0 & 0 \end{pmatrix} \begin{Bmatrix} l & F & T \\ F' & l' & 4 \end{Bmatrix} Q(f,f',F,F',i), \tag{30}$$

$$F_6(l,l',f,f',F,F',T,i) = (-1)^{F+T} \sum_{K=0,2,4} \nu_K \begin{Bmatrix} l & F & T \\ F' & l' & K \end{Bmatrix} \begin{pmatrix} l' & K & l \\ 0 & 0 & 0 \end{pmatrix} I_K(f,f',F,F',i), \tag{31}$$

and $\nu_0 = \frac{12}{\sqrt{5}}$, $\nu_2 = -12\sqrt{\frac{2}{7}}$, and $\nu_4 = 36\sqrt{\frac{2}{35}}$. We can see F_3 only includes the magnetic dipole-dipole interaction, F_5 completely arises from the electronic quadrupole-quadrupole interaction, and all van der Waals dispersion effects are involved in F_6. Additionally, for the interatomic interaction $V_{\rm int}(r)$, the total angular momentum T and its projection M_T on the space-fixed axis are two conserved quantities.

The matrix elements of the molecular rotation can be expressed as

$$\langle\alpha|\frac{\mathbf{L}^2}{2mr^2}|\alpha'\rangle = \delta_{l,l'}\delta_{f,f'}\delta_{F,F'}\delta_{T,T'}\delta_{M_T,M_T'}\frac{l(l+1)}{2mr^2}, \tag{32}$$

and the matrix elements of the hyperfine interaction of fermionic ^{87}Sr are given by

$$\langle\alpha|H_{\rm hpf}(b)|\alpha'\rangle = \delta_{l,l'}\delta_{f,f'}\delta_{F,F'}\delta_{T,T'}\delta_{M_T,M_T'}\left\{A\left(f(f+1)-\frac{123}{4}\right)+\frac{B}{432}\left[\left(f(f+1)-\frac{123}{4}\right)^2-\frac{297}{2}\right]\right\}, \tag{33}$$

where the hyperfine interaction constants [25] for the $(5s5p)\,^3P_2$ state of ^{87}Sr are $A = -212.765$ MHz and $B = 67.215$ MHz. Thus, we obtain all the elements of Hamiltonian H in the representation of the space-fixed fragmentation channels $\{|\alpha\rangle\}$.

III. ULTRACOLD COLLISIONS OF TWO ATOMS IN THE FREE SPACE

Now we consider ultracold collisions between two metastable ^{88}Sr and ^{87}Sr atoms in the free space. First, we investigate the diatomic system in the adiabatic approximation, which can provide a qualitative description of the two-body scattering with anisotropic interatomic interactions. Then we consider the elastic and inelastic scattering rates by solving the system of coupled radial Schrödinger equations.

A. Adiabatic potential-energy curves

The adiabatic potential-energy curves can be derived by diagonalizing the matrix $\frac{\mathbf{L}^2}{2mr^2} + V_{\rm int}(r) + H_{\rm hpf}(b)$. Since no external magnetic field is applied to the diatomic system, the total angular momentum T and its projection M_T on the space-fixed axis are conserved at all stages of collisions between two metastable atoms. Thus, the adiabatic potential-energy curves can be classified by (T, M_T). Based on Eq. (28), we find that at interatomic distances within the range from $50a_0$ to $100a_0$, energies of electric dipole-dipole and quadrupole-quadrupole interactions are of the order of 10^{-7}–10^{-8} rydberg, which are comparable with the hyperfine-structure splitting of the metastable $(5s5p)\,^3P_2$ level of ^{87}Sr, and the magnetic dipole-dipole interaction is of the order of 10^{-9} rydberg. Collision channels with different quantum numbers f_b are strongly coupled to each other in this region due to the anisotropic interatomic interactions, as shown in Fig. 1. When the interatomic distance is larger than $100a_0$, the adiabatic potential-energy curves converge to five different dissociation limits, which correspond to five hyperfine-structure levels of fermionic ^{87}Sr. In addition, at interatomic distances larger than $50a_0$, the interatomic interactions are unable to distort the spin-orbit coupling patterns in ^{88}Sr and ^{87}Sr. The formalism established in Sec. II is still useful for the quantitative description.

In experiments, it is easy to prepare two atoms in fully polarized s-wave entrance channels. For example, if two atoms are initially prepared in $|\xi, j = 2, m_j = 2\rangle_a$ and $|\xi, j, i, f, m_f = f\rangle_b$ states to the dissociation limit ($r \to \infty$) and in a rotational s-wave state $|l = 0, m_l = 0\rangle$, the only allowed entrance channel in the coupled representation is

$$|\Sigma = F\rangle = |l = 0, (\xi, j)_a, (\xi, j, i, f)_b, F = j + f, T = F, M_T = F\rangle, \tag{34}$$

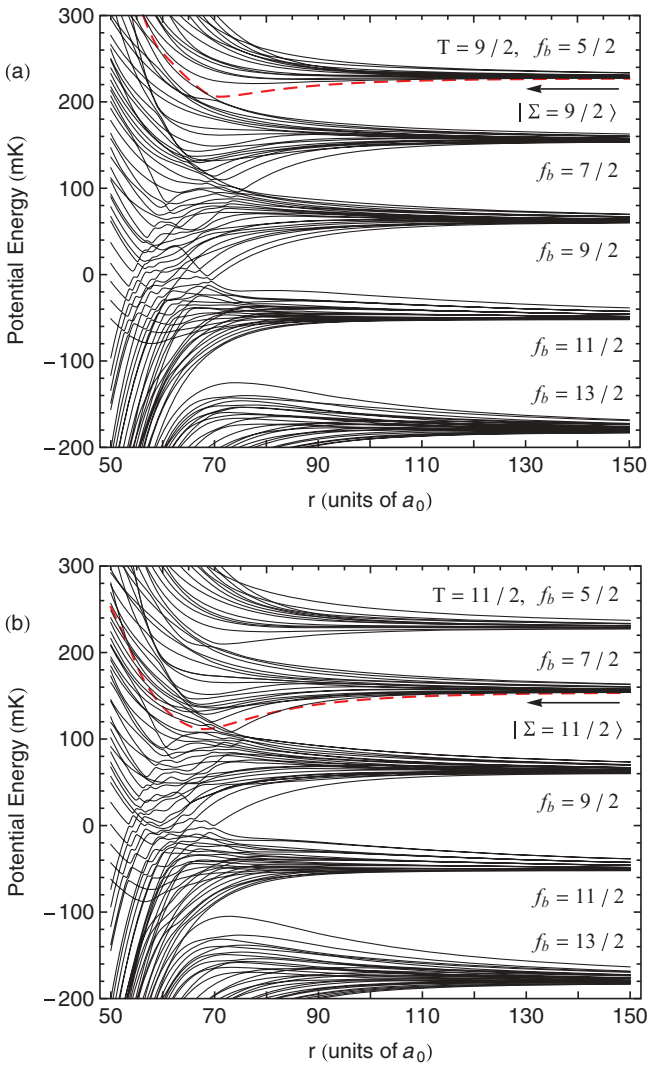

FIG. 1. (Color online) Ultracold collisions between two metastable strontium atoms $(5s5p)\,^3P_2$ and $(5s5p)\,^3P_2$ ($i = \frac{9}{2}$) in the free space. (a) Adiabatic potential-energy curves for $(T = \frac{9}{2}, M_T = \frac{9}{2})$. The maximum partial wave taken into account for these curves is $l_{\rm max} = 20$. The fully polarized s-wave entrance channel $|\Sigma = \frac{9}{2}\rangle$ is marked by a big arrow, and the corresponding curve (dashed line) presents a long-range molecular potential well at the distance of $r \sim 70a_0$. All the asymptotes are marked by the quantum number f_b. (b) Adiabatic potential-energy curves for $(T = \frac{11}{2}, M_T = \frac{11}{2})$. The potential-energy curve (dashed line) for the entrance channel $|\Sigma = \frac{11}{2}\rangle$ is marked by a big arrow.

which can be further written in a decoupled form,

$$|\Sigma = F\rangle = |l=0,m_l=0\rangle|\xi,j,m_j=2\rangle_a|\xi,j,i,f,m_f=f\rangle_b. \quad (35)$$

For our diatomic system, two atoms can be prepared in five fully polarized s-wave entrance channels $|\Sigma = \frac{9}{2},\frac{11}{2},\frac{13}{2},\frac{15}{2},\frac{17}{2}\rangle$ in experiments.

Figure 1(a) displays all the adiabatic potential-energy curves for a total angular momentum of $T = \frac{9}{2}$ and a projection of $M_T = \frac{9}{2}$. The partial waves up to the maximum of $l_{\max} = 20$ are taken into account. The fully polarized s-wave entrance channel $|\Sigma = \frac{9}{2}\rangle = |l=0,(\xi,j)_a,(\xi,j,i,f=\frac{5}{2})_b,F=\frac{9}{2},T=\frac{9}{2},M_T=\frac{9}{2}\rangle$ has been marked by a big arrow. As one can see, there exist numerous avoided crossings at interatomic distances in the range of $50a_0 < r < 70a_0$ since the electric quadrupole-quadrupole interaction plays a major role in this region. The key feature in Fig. 1(a) is the pronounced avoided crossing at $r \sim 70a_0$, primarily formed by the entrance-channel curve and a curve converging to a lower dissociation limit with $|l=10,(\xi,j)_a,(\xi,j,i,f=\frac{7}{2})_b,F=\frac{11}{2},T=\frac{9}{2},M_T=\frac{9}{2}\rangle$. This avoided crossing leads to a long-range molecular potential well in the entrance-channel curve. Similarly, for two atoms in the entrance channel $|\Sigma = \frac{11}{2}\rangle = |l=0,(\xi,j)_a,(\xi,j,i,f=\frac{7}{2})_b,F=\frac{11}{2},T=\frac{11}{2},M_T=\frac{11}{2}\rangle$, a deeper long-range molecular potential well can be found in the entrance-channel curve due to the pronounced avoided crossing at $r \sim 70a_0$, as shown in Fig. 1(b). This avoided crossing is mostly formed between the entrance-channel curve and a curve converging to a dissociation limit with $|l=10,(\xi,j)_a,(\xi,j,i,f=\frac{9}{2})_b,F=\frac{9}{2},T=\frac{11}{2},M_T=\frac{11}{2}\rangle$.

Other important information we can obtain from Fig. 1 is that at interatomic distances $r < 60a_0$ the repulsive potential, which is much larger than the relative collision energy of two atoms at ultracold temperatures (<10 μK), dominates the two-body collisions in both entrance channels $|\Sigma = \frac{9}{2}\rangle$ and $|\Sigma = \frac{11}{2}\rangle$. Thus, almost no atomic flux can penetrate into the inner region ($r < 50a_0$), and the two-body scattering is mainly governed by long-range interatomic interactions. In the adiabatic approximation, we numerically compute the bound states and probability distributions of two atoms in two entrance-channel potential wells by applying the well-known Numerov method. As shown in Fig. 2, the potential well in the entrance channel $|\Sigma = \frac{9}{2}\rangle$ can hold only one bound state, while two bound states exist in the deeper potential well in the entrance channel $|\Sigma = \frac{11}{2}\rangle$.

In addition to $(T=\frac{9}{2},M_T=\frac{9}{2})$ and $(T=\frac{11}{2},M_T=\frac{11}{2})$, we have also computed the adiabatic potential-energy curves for the total angular momentums of $(T=\frac{13}{2},\frac{15}{2},\frac{17}{2})$ and the corresponding projections of $(M_T=\frac{13}{2},\frac{15}{2},\frac{17}{2})$. For simplicity, we do not show them here. Unlike the potential-energy curves for entrance channels $|\Sigma = \frac{9}{2},\frac{11}{2}\rangle$ in the adiabatic approximation, the attractive interactions dominate ultracold collisions of two atoms in entrance channels $|\Sigma = \frac{13}{2},\frac{15}{2},\frac{17}{2}\rangle$ at the interatomic distance of about $50a_0$, and no long-range potential wells exist in the entrance-channel curves. In this case, we have to involve the short-range interatomic interactions of two atoms in entrance channels $|\Sigma = \frac{13}{2},\frac{15}{2},\frac{17}{2}\rangle$. Unfortunately, we do not have the relevant data. In the following discussion we are going to concentrate on ultracold collisions of two atoms in entrance channels $|\Sigma = \frac{9}{2}\rangle$ and $|\Sigma = \frac{11}{2}\rangle$.

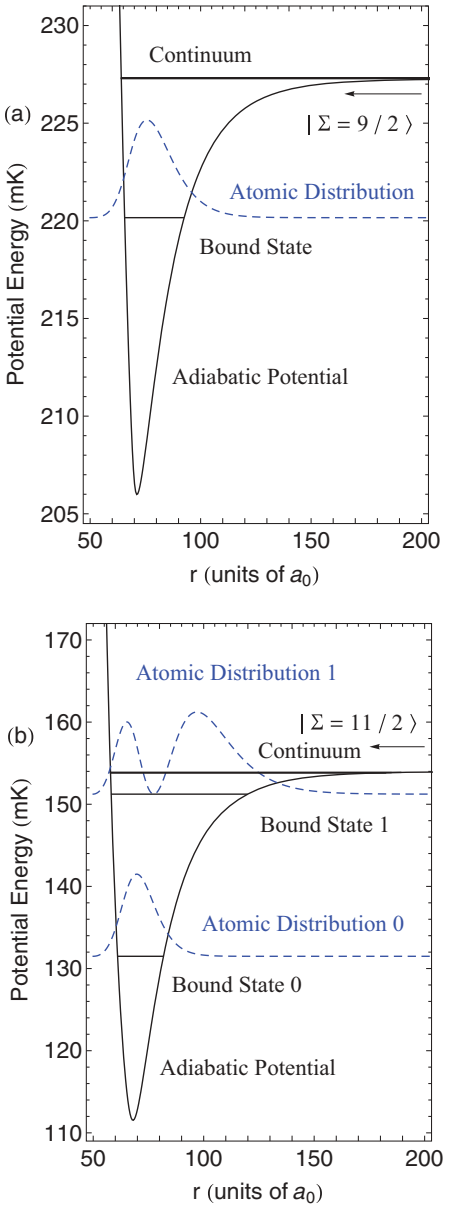

FIG. 2. (Color online) Adiabatic potential-energy curves for entrance channels (a) $|\Sigma = \frac{9}{2}\rangle$ and (b) $|\Sigma = \frac{11}{2}\rangle$. The potential well in the entrance channel $|\Sigma = \frac{9}{2}\rangle$ can hold only one bound state while two bound states exist in the deeper potential well in the entrance channel $|\Sigma = \frac{11}{2}\rangle$. The corresponding atomic distributions have been marked.

B. The diabatic description of two-body collisions

Above, we have considered the adiabatic potential-energy curves of ultracold collisions between two metastable ^{88}Sr and ^{87}Sr atoms. However, this adiabatic approximation can only give a qualitative description of the two-body scattering with anisotropic interatomic interactions. In order to implement a quantitative analysis, especially to obtain the elastic and inelastic scattering rates, we have to solve the system of coupled radial Schrödinger equations in the diabatic representation,

which relies on the fact that all diagonal and nondiagonal elements of Hamiltonian H vary smoothly with the interatomic distance r.

By substituting $\psi_\alpha(E,\mathbf{r})$ into the stationary Schrödinger equation and applying the Hamiltonian in Eq. (1), one can obtain a set of coupled radial Schrödinger equations for a given asymptotic collision energy E in an entrance channel $|\alpha\rangle$. Here we apply the multichannel log-derivative method [26] to numerically solve the coupled radial Schrödinger equations. The standard boundary conditions imposed on $\phi_{\alpha',\alpha}(E,r)$ for a scattering state $|\alpha'\rangle$ are $\phi_{\alpha',\alpha}(E,r\to 0)\to 0$ and

$$\phi_{\alpha',\alpha}(E,r) = J_{\alpha',\alpha}(k_{\alpha'}r) + \sum_{\alpha''} N_{\alpha',\alpha''}(k_{\alpha''}r)K_{\alpha'',\alpha}, \quad (36)$$

where we have defined the channel wave number $k_\alpha = \sqrt{2m\Delta E_\alpha}/\hbar$ and the relative kinetic energy $\Delta E_\alpha = E - E_\alpha$. Since the interatomic potentials at $r\sim 50a_0$ in entrance channels $|\Sigma = \frac{9}{2},\frac{11}{2}\rangle$ are positive and much larger than the relative collision energy of two atoms at ultracold temperatures ($<10\,\mu$K) as shown in Fig. 1, the minimal interatomic distance in this paper is chosen to be $r_{\min} = 50a_0$. Thus, the boundary condition at the short-range interatomic distance should be modified as $\phi_{\alpha',\alpha}(E,r\to 50)\to 0$.

Channels with thresholds greater than E are said to be closed; otherwise, they are open. The matrices $\mathbf{J} = (J_{\alpha,\alpha'})$ and $\mathbf{N} = (N_{\alpha,\alpha'})$ are diagonal matrices, whose matrix elements for the open channels are made up of Riccati-Bessel functions and of modified spherical Bessel functions for the closed channels. The well-known scattering $\mathbf{S} = (S_{\alpha,\alpha'})$ matrix is related to the open-open submatrix $\mathbf{K}_{oo}$ of $\mathbf{K} = (N_{\alpha,\alpha'})$ by

$$\mathbf{S} = (1 + i\mathbf{K}_{oo})^{-1}(1 - i\mathbf{K}_{oo}). \quad (37)$$

Once we obtain the scattering S matrix, the elastic (el) and inelastic (inel) scattering rates of atoms in the entrance channel $|\alpha\rangle$ can be calculated straightforwardly by the formulas $\Gamma_\alpha^{\rm el} = \frac{\pi\hbar}{mk_\alpha}|S_{\alpha,\alpha} - \delta_{\alpha,\alpha}|^2$ and $\Gamma_\alpha^{\rm inel} = \sum_{\alpha'\neq\alpha}\frac{\pi\hbar}{mk_\alpha}|S_{\alpha',\alpha} - \delta_{\alpha',\alpha}|^2$, respectively. Moreover, the inelastic processes and the resulting loss from the entrance channel $|\alpha\rangle$ of interest are more appropriately described by an energy-dependent complex scattering length [27],

$$\tilde{a}\,(|\alpha\rangle,\Delta E_\alpha) = a_{r,\alpha} + i a_{i,\alpha} \equiv -\frac{1}{k_\alpha^{2l+1}}\tan\left(\frac{\ln S_{\alpha,\alpha}}{2i}\right), \quad (38)$$

where the real part $a_{r,\alpha}$ of the complex scattering length corresponds to the usual elastic scattering length, while the imaginary part $a_{i,\alpha}$ is a measure of the loss from the scattering channel $|\alpha\rangle$ to all other open channels. We should note that since the atomic temperature achieved in experiments is not absolutely in the zero-energy limit, we need to consider the energy-dependent complex scattering length [28] here, which will be also used in next section, rather than the zero-energy one.

By solving the coupled radial Schrödinger equations within the range from $r_{\min} = 50a_0$ to $r_{\max} = 2500a_0$, we derived the elastic and inelastic scattering rates of atoms in entrance channels $|\Sigma = \frac{9}{2},\frac{11}{2}\rangle$ as a function of the relative collision energy ΔE, as shown in Fig. 3. (We have verified that our results, especially the calculated S matrix, are converged with respect to variations of the integration limits $r_{\min}$ and $r_{\max}$.) As one can see, the inelastic scattering dominates ultracold collisions of atoms in both entrance channels and leads to the large inelastic losses. It coincides with what we have pointed out in Sec. I that although an avoided crossing can produce an adiabatic potential well in a fully polarized s-wave entrance channel, the strong coupling between different scattering partial waves and electronic degrees of freedom by long-range anisotropic interatomic interactions can lead to severe depolarization of atoms and thus to inelastic losses. In addition, at relative collision energies $\Delta E < 10\ \mu$K, the complex s-wave scattering lengths of atoms in entrance channels $|\Sigma = \frac{9}{2},\frac{11}{2}\rangle$ are $\tilde{a}(|\Sigma = \frac{9}{2}\rangle,\Delta E)\approx(165 + i86)a_0$ and $\tilde{a}(|\Sigma = \frac{11}{2}\rangle,\Delta E)\approx(91 + i116)a_0$, respectively. (Here we should note that at a relative collision energy ΔE lower than 10 μK the difference between $\tilde{a}(|\Sigma\rangle,\Delta E < 10\mu\text{K})$ and the zero-energy complex scattering length $\tilde{a}(|\Sigma\rangle,\Delta E\approx 0)$ is smaller than 0.5%.) In each entrance channel, the imaginary part of the complex scattering length is close to (or even larger than) the real part, which, again, means a high inelastic loss of atoms in the entrance channel. We conclude this section by remarking that in the free space without external magnetic field, the two-body scattering between metastable ^{88}Sr and ^{87}Sr is governed by the long-range anisotropic interatomic interactions, which leads to the strong coupling between different partial waves and results in a high rate of inelastic losses.

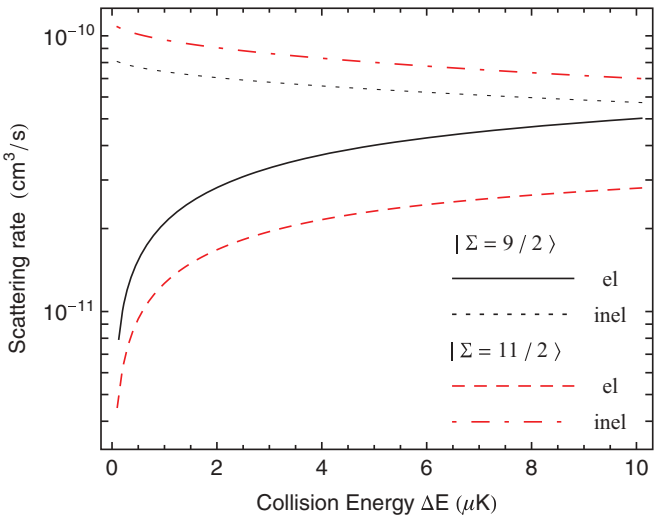

FIG. 3. (Color online) The elastic and inelastic scattering rates of atoms in entrance channels $|\Sigma = \frac{9}{2}\rangle$ and $|\Sigma = \frac{11}{2}\rangle$ as a function of the relative incident kinetic energy ΔE. In general, the atomic temperature available in experiments is in the range from 0.1 to 10 μK.

IV. TWO-BODY COLLISIONS IN AN EXTERNAL MAGNETIC FIELD

Above we have considered ultracold collisions of atoms in the free space. Now we consider the effect of an external static magnetic field $\mathbf{B}_0 = \mathcal{B}_0\mathbf{e}_z$ ($\mathbf{e}_z$ is the z direction in the space-fixed frame) on the two-body collisions. The element of

Zeeman interaction

$$H_z = -\left(\boldsymbol{\mu}^{(1_a)} + \boldsymbol{\mu}^{(1_b)}\right) \cdot \mathbf{B}_0 \tag{39}$$

of the atomic magnetic dipole momentums with the external magnetic field $\mathbf{B}_0$ is given by

$$\begin{aligned}\langle \alpha | H_z | \alpha' \rangle = {} & (-1)^{2T-M_T+l+F'} \delta_{l,l'} \delta_{M_T,M_T'} \frac{\sqrt{30}}{2} \sqrt{[F,T,F',T']} \begin{pmatrix} T & 1 & T' \\ -M_T & 0 & M_T \end{pmatrix} \begin{Bmatrix} T & 1 & T' \\ F' & 1 & F \end{Bmatrix} \\ & \times \left[(-1)^{f+F'} \delta_{f,f'} \begin{Bmatrix} F & 1 & F' \\ 2 & f & 2 \end{Bmatrix} g_{ls} - (-1)^{\frac{9}{2}+f'+F} \sqrt{[f,f']} \begin{Bmatrix} F & 1 & F' \\ f' & 2 & f \end{Bmatrix} \left((-1)^{f'} \begin{Bmatrix} f & 1 & f' \\ 2 & \frac{9}{2} & 2 \end{Bmatrix} g_{ls} \right.\right. \\ & \left.\left. + (-1)^{f} \sqrt{33} \begin{Bmatrix} f & 1 & f' \\ \frac{9}{2} & 2 & \frac{9}{2} \end{Bmatrix} g_i \right) \right] \mu_B \mathcal{B}_0. \end{aligned} \tag{40}$$

As one can see, the existence of magnetic field $\mathbf{B}_0$ breaks the local rotational invariance, and the total angular momentum T is no longer a good quantum number. In Ref. [17], it is pointed out that electronic states with different F do not couple with each other in the case of identical atoms. However, this conclusion does not hold true for two nonidentical atoms, as shown in Eq. (40), which reduces the symmetry of the diatomic system.

Due to the Zeeman interaction H_z, two atoms cannot be completely prepared in a certain fully polarized s-wave entrance channel. In this case, we need to consider to what extent the external magnetic field does not affect much the preparation of atoms in the entrance channel $|\Sigma\rangle$. We assume that two metastable atoms are initially completely prepared in $|\Sigma\rangle$ at the zero magnetic field $\mathcal{B}_0 = 0$. Then we turn on the magnetic field and check the probability of atoms remaining in $|\Sigma\rangle$. Figure 4 displays the normalized number of atoms remaining in $|\Sigma\rangle$ as a function of the strength of magnetic field $\mathcal{B}_0$. For $|\Sigma = \frac{9}{2}\rangle$, the larger $\mathcal{B}_0$ transfers more atoms to other collision channels, but atoms still have more than a 98% probability of remaining in the entrance channel $|\Sigma = \frac{9}{2}\rangle$ at magnetic fields $\mathcal{B}_0 < 100$ gauss. For other entrance channels $|\Sigma = \frac{11}{2}, \frac{13}{2}, \frac{15}{2}, \frac{17}{2}\rangle$, the dependence of the preparation of atoms on the magnetic field $\mathcal{B}_0$ becomes weaker; in particular, the magnetic field $\mathcal{B}_0$ does not transfer any atoms in $|\Sigma = \frac{17}{2}\rangle$ to other collision channels since the Zeeman interaction H_z keeps the quantum number l conserved.

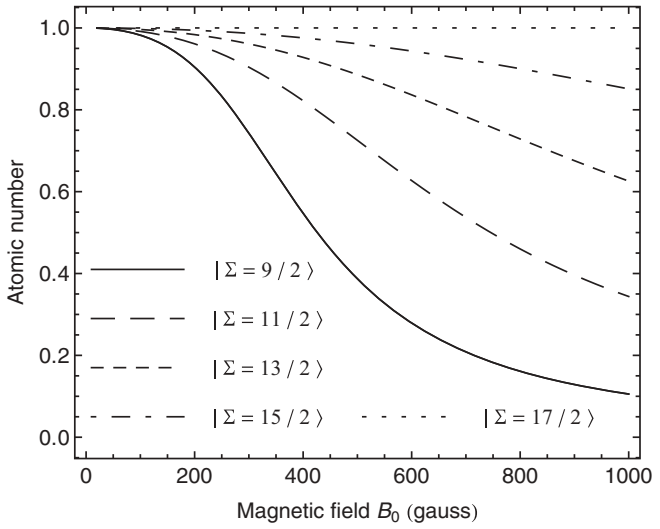

FIG. 4. The normalized number of two atoms initially prepared in different entrance channels $|\Sigma\rangle$ as a function of the external magnetic field $\mathcal{B}_0$.

Now we investigate the magnetic-field dependence of the energy-dependent complex s-wave scattering lengths and the elastic and inelastic scattering rates of atoms in entrance channels $|\Sigma = \frac{9}{2}, \frac{11}{2}\rangle$ based on the coupled multichannel-scattering calculation. Here we focus on the ultracold collisions at a temperature as low as 1 μK, which is available in experiments. As shown in Fig. 5(a), the complex scattering length in the entrance channel $|\Sigma = \frac{9}{2}\rangle$ strongly depends on the weak magnetic field and displays a resonance behavior, which is associated with inelastic processes, at $\mathcal{B}_0 \approx 8.7$ gauss. A similar resonance behavior can be found at $\mathcal{B}_0 \approx 11.1$ gauss in the entrance channel $|\Sigma = \frac{11}{2}\rangle$. Around each resonance, the imaginary part of the complex scattering length is several orders smaller than the real part. In this resonance regime, couplings to other collision channels due to long-range anisotropic interactions can be neglected, which implies that the interatomic interaction between two atoms in the entrance channel $|\Sigma = \frac{9}{2}\rangle$ or $|\Sigma = \frac{11}{2}\rangle$ can be treated to good approximation as a single channel scattering. Additionally, we find that in the regime of $25 < \mathcal{B}_0 < 100$ gauss no such a resonance exists in both entrance channels.

The corresponding dependence of the elastic and inelastic scattering rates on the magnetic field is shown in Fig. 5(b). Increasing $\mathcal{B}_0$ can suppress the inelastic scattering and enlarge elastic scattering rates because the incident and outgoing channels, which have the same quantum number f_b, are well separated and the Zeeman effect can eliminate many avoided crossings at the long-range interatomic distances. In each resonance regime the elastic scattering rate is much larger than the inelastic one, which coincides with the complex scattering lengths in Fig. 5(a). However, after each resonance regime there exists a certain $\mathcal{B}_0$ at which the real part of the complex scattering length is zero $a_r = 0$. Passing this point, the elastic scattering rate first strongly decreases and then increases again. Additionally, we find that for two interacting atoms in entrance channels $|\Sigma = \frac{9}{2}, \frac{11}{2}\rangle$ the elastic scattering rates are always larger than the inelastic scattering rates in the regime of $25 < \mathcal{B}_0 < 100$ gauss.

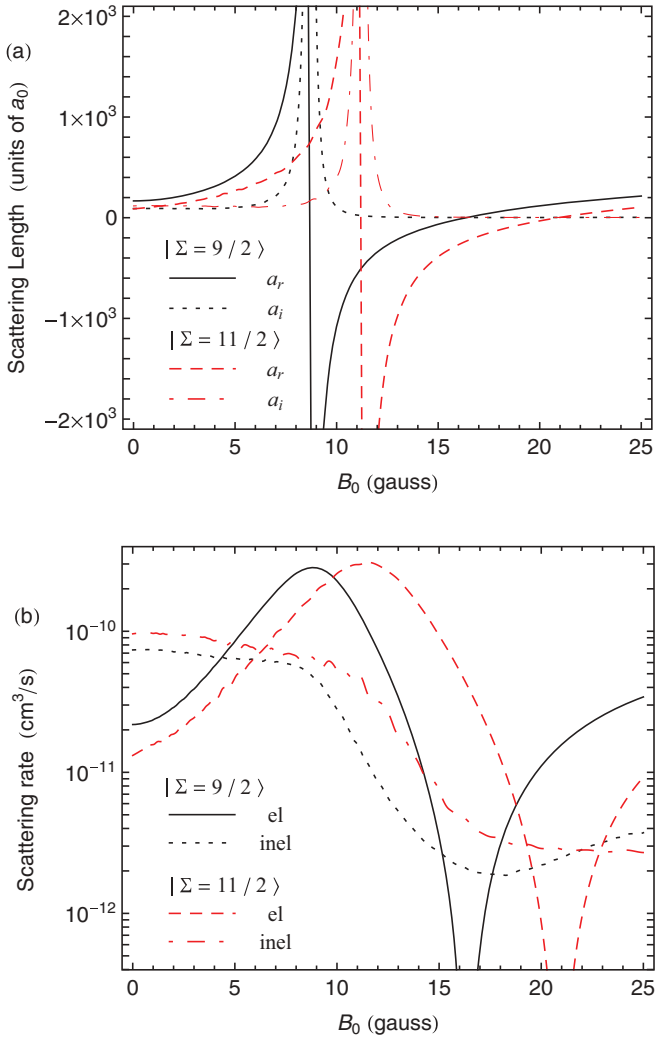

FIG. 5. (Color online) Magnetic-field effect. (a) The dependence of the energy-dependent complex s-wave scattering lengths as a function of magnetic field $\mathcal{B}_0$ at a relative collision energy of $\Delta E = 1\ \mu$K. (b) The corresponding elastic and inelastic scattering rates changing with $\mathcal{B}_0$. In the coupled multichannel-scattering calculation, the maximum partial wave taken into account for these curves is $l_{\max} = 20$.

We should note that at different relative collision energies ΔE, the dependence of the energy-dependent complex scattering length and the elastic and inelastic scattering rates on the magnetic field will be different. For example, we find that at a relative collision energy of $\Delta E = 10\ \mu$K there are two certain values of $\mathcal{B}_0$ at which the complex scattering length behaves resonantly in both entrance channels $|\Sigma = \frac{9}{2}\rangle$ and $|\Sigma = \frac{11}{2}\rangle$. Since the atomic temperature available in experiments can be as low as 1 μK, here we only focus on the ultracold collisions in this low-temperature regime.

V. TWO INTERACTING ATOMS IN AN OPTICAL LATTICE SITE

So far, we have studied ultracold collisions of atoms without extra confinement. Now, we consider the system of two atoms confined in an optical lattice site. In order to eliminate the anisotropy induced by the optical lattice, here we choose a three-dimensional optical lattice formed by three orthogonal standing waves along the directions

$$\boldsymbol{\epsilon}_1 = \frac{1+\sqrt{3}}{2\sqrt{3}}\mathbf{e}_x + \frac{1-\sqrt{3}}{2\sqrt{3}}\mathbf{e}_y - \frac{1}{\sqrt{3}}\mathbf{e}_z, \tag{41}$$

$$\boldsymbol{\epsilon}_2 = \frac{1-\sqrt{3}}{2\sqrt{3}}\mathbf{e}_x + \frac{1+\sqrt{3}}{2\sqrt{3}}\mathbf{e}_y - \frac{1}{\sqrt{3}}\mathbf{e}_z, \tag{42}$$

$$\boldsymbol{\epsilon}_3 = \frac{1}{\sqrt{3}}\mathbf{e}_x + \frac{1}{\sqrt{3}}\mathbf{e}_y + \frac{1}{\sqrt{3}}\mathbf{e}_z \tag{43}$$

and linearly polarized along $\boldsymbol{\epsilon}_3$, $\boldsymbol{\epsilon}_1$, and $\boldsymbol{\epsilon}_2$, respectively. ($\mathbf{e}_{x,y,z}$ are three unit vectors in the Cartesian coordinate system.) Three polarizations have relations $\boldsymbol{\epsilon}_i \cdot \boldsymbol{\epsilon}_j = \delta_{i,j}$, $\boldsymbol{\epsilon}_1 \times \boldsymbol{\epsilon}_2 = \boldsymbol{\epsilon}_3$, $\boldsymbol{\epsilon}_2 \times \boldsymbol{\epsilon}_3 = \boldsymbol{\epsilon}_1$, and $\boldsymbol{\epsilon}_3 \times \boldsymbol{\epsilon}_1 = \boldsymbol{\epsilon}_2$. The lattice field in the space-fixed frame can be expressed as

$$\begin{aligned}\mathbf{E}(\omega_L,t) = 2\mathcal{E}_L \{&\boldsymbol{\epsilon}_1 \cos(k_L \boldsymbol{\epsilon}_2 \cdot \mathbf{r}) \cos[\omega_L t + \varphi_1(t)] \\ &+ \boldsymbol{\epsilon}_2 \cos(k_L \boldsymbol{\epsilon}_3 \cdot \mathbf{r}) \cos[\omega_L t + \varphi_2(t)] \\ &+ \boldsymbol{\epsilon}_3 \cos(k_L \boldsymbol{\epsilon}_1 \cdot \mathbf{r}) \cos[\omega_L t + \varphi_3(t)]\},\end{aligned} \tag{44}$$

where $\mathcal{E}_L$, ω_L, and $k_L = 2\pi/\lambda_L$ are the amplitude, frequency, and wave number of the lattice field, respectively. The noise phases $\varphi_i(t)$ are introduced so as to eliminate the interference effect between different standing waves, i.e., $\langle \cos[\varphi_i(t) - \varphi_j(t)] \rangle_t = \delta_{i,j}$, where $\langle \cdots \rangle_t$ denotes the time average. Thus, three standing waves are independent, and the ac Stark shift of an atomic state is equal to the sum of light shifts induced by each standing wave.

A. ac Stark shift

For a fine-structure $|\xi, j, m_j\rangle_a = (5s5p)\,^3P_2(m_j)$ state of ^{88}Sr, its ac Stark shift induced by the far-off-resonance lattice field is given by

$$U_{m_j}(\lambda_L, I_L) = -2c\mu_0 I_L \alpha_{m_j}(\lambda_L) D(x,y,z), \tag{45}$$

where the induced atomic polarizability

$$\alpha_{m_j}(\lambda_L) = \sum_{\xi',j'} \frac{2\pi\varepsilon_0 c^3 A_{(\xi',j'),(\xi,j)}}{\omega^2_{(\xi',j'),(\xi,j)}\left(\omega^2_{(\xi',j'),(\xi,j)} - \omega_L^2\right)} \frac{[j']}{[2]} \tag{46}$$

can be derived from the method in Ref. [29], $I_L = \mathcal{E}_L^2/(2c\mu_0)$ is the intensity of lattice field, and the distribution of the optical lattice potential is described by the function

$$D(x,y,z) = \sum_i \sin^2(k_L \boldsymbol{\epsilon}_i \cdot \mathbf{r}). \tag{47}$$

(ξ, j) stands for the fine-structure $(5s5p)\,^3P_2$ level, while (ξ', j') denotes any other fine-structure levels that are electric-dipole transition allowed between (ξ, j) and (ξ', j'), such as $^3S_1$ and $^3D_{1,2,3}$. $\omega_{(\xi',j'),(\xi,j)}$ is the frequency of the atomic $(\xi', j') \to (\xi, j)$ transition. The respective Einstein coefficients $A_{(\xi',j'),(\xi,j)}$ from the upper (ξ', j') level to the lower (ξ, j) level can be found in Ref. [30]. From Eq. (46), one can

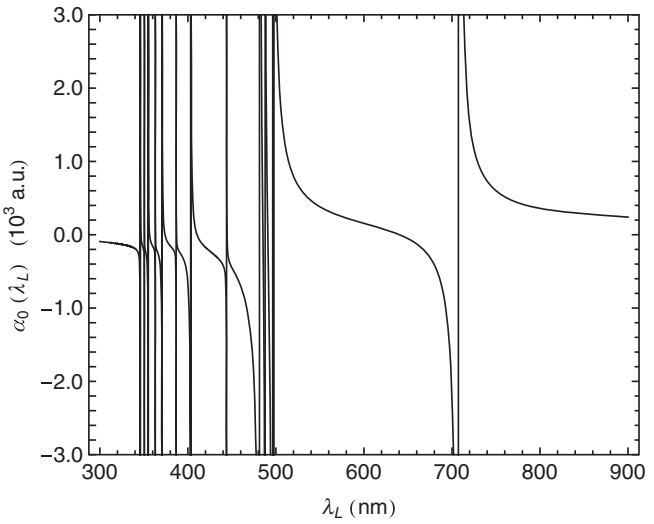

FIG. 6. The induced atomic polarizability $\alpha_0(\lambda_L)$ as a function of the wavelength λ_L of the optical lattice field.

see that due to the full symmetry of optical lattice the light shift of the $|\xi,j,m_j\rangle$ state is unrelated to the projection m_j of the total angular momentum j. We can simplify $\alpha_{m_j}(\lambda_L)$ as $\alpha_0(\lambda_L)$.

Similarly, the ac Stark shift of a hyperfine-structure $|\xi,j,i,f,m_f\rangle_b = (5s5p)\,^3P_2(f,m_f)$ state of ^{87}Sr reads

$$U_{f,m_f}(\lambda_L,I_L) = -2c\mu_0 I_L \alpha_f(\lambda_L) D(x,y,z), \tag{48}$$

where the induced atomic polarizability

$$\alpha_f(\lambda_L) = \sum_{\xi',j',f'} \frac{2\pi\varepsilon_0 c^3 A_{(\xi',j'),(\xi,j)}[f'][j']}{\omega^2_{(\xi',j',f'),(\xi,j,f)}\left(\omega^2_{(\xi',j',f'),(\xi,j,f)} - \omega_L^2\right)} \times \begin{Bmatrix} j' & \frac{9}{2} & f' \\ f & 1 & j \end{Bmatrix}^2 \tag{49}$$

and $\omega_{(\xi',j',f'),(\xi,j,f)}$ is the frequency of the atomic $(\xi',j',f') \to (\xi,j,f)$ transition. Since the frequency ω_L of the lattice field is far off resonance to any $(\xi',j',f') \to (\xi,j,f)$ transitions, one can ignore the effect of hyperfine splitting on the light shift, i.e., $\omega_{(\xi',j',f'),(\xi,j,f)} \approx \omega_{(\xi',j'),(\xi,j)}$, which leads to $\alpha_f(\lambda_L) \approx \alpha_0(\lambda_L)$.

We arrive at a conclusion that the optical lattice field does not change the relative frequency differences between any two atomic hyperfine-structure states of ^{87}Sr, and the lattice potential for each fine-structure sublevel of ^{88}Sr and hyperfine sublevel of ^{87}Sr is given by $U(\mathbf{r}) = U_0(\lambda_L,I_L)D(x,y,z)$, where we have defined $U_0(\lambda_L,I_L) = -2c\mu_0\alpha_0(\lambda_L)I_L$. Figure 6 displays the induced atomic polarizability $\alpha_0(\lambda_L)$ changing with the wavelength of the optical lattice field. For the red-detuned optical lattice usually used for strontium in experiments, whose wavelength is about $\lambda_L = 813.4$ nm and lattice constant is $\lambda_L/2$, we have $\alpha_0(\lambda_L) = 334.6$ a.u.

B. Harmonic approximation

Now we consider two interacting atoms in an optical lattice with a wavelength of $\lambda_L = 813.4$ nm. The Hamiltonian describing two atoms with coordinate vectors $\mathbf{r}_a$ and $\mathbf{r}_b$ in a three-dimensional optical lattice is expressed as

$$H(\mathbf{r}_a,\mathbf{r}_b) = \frac{\mathbf{p}_a^2}{2m_a} + \frac{\mathbf{p}_b^2}{2m_b} + U(\mathbf{r}_a) + U(\mathbf{r}_b) + V_{\rm int}(\mathbf{r}_a,\mathbf{r}_b), \tag{50}$$

where $\mathbf{p}^2_{a,b}/(2m_{a,b})$ are the kinetic energy operators for atoms a and b, U is the sinusoidal trapping potential, and $V_{\rm int}$ is the interatomic interaction. It is convenient for us to treat the two-body problem in center-of-mass (c.m.) and relative (RL) motion coordinates.

Assuming a sufficiently strong optical lattice, the lowest-energy state of a lattice cell is approximated by the harmonic oscillator ground state. For the reduced atomic mass $m = m_a m_b/(m_a+m_b)$ and lattice potential U_0, one can define the single-site harmonic oscillator frequency $\omega_h = k_L\sqrt{-U_0/m}$. The extent of the harmonic oscillator ground state is given by $d_h = \sqrt{\hbar/(m\omega_h)}$, and the localization at a lattice site is quantified by the Lamb-Dicke parameter $\eta = k_L d_h$. We normally assume that atoms are in the Lamb-Dicke regime $\eta \ll 1$ and each optical lattice site traps one ^{88}Sr atom and one ^{87}Sr atom. By defining the c.m. coordinate $\mathbf{R} = \mathbf{r}_a + \mathbf{r}_b$ and the RL coordinate $\mathbf{r} = \mathbf{r}_a - \mathbf{r}_b$, two interacting atoms in an optical lattice site can be described by the decoupled c.m. and RL coordinate Hamiltonians,

$$H_{\rm c.m.} = \frac{\mathbf{P}_R^2}{2M} + \frac{1}{2}M\omega_h^2 R^2, \tag{51}$$

$$H_{RL} = \frac{\mathbf{p}_r^2}{2m} + \frac{1}{2}m\omega_h^2 r^2 + V_{\rm int}(r) + H_{\rm hpf}(b), \tag{52}$$

in the harmonic approximation, where $M = m_a + m_b$ is the total mass and we have added the hyperfine interaction of ^{87}Sr in Eq. (52). Comparing Eq. (1) with Eq. (52), the only difference is the term of extra isotropic harmonic potential $U_{RL}(r) = \frac{1}{2}m\omega_h^2 r^2$.

Generally, the intensity of lattice field I_L applied in experiments is chosen to be 10 kW/cm^2, which gives an optical lattice potential of $U_0 = -30$ μK and the harmonic oscillator frequency of $\omega_h = 2\pi \times 65.8$ kHz. The characteristic length of the harmonic trap, i.e., the extent of harmonic oscillator ground state, is about $d_h = 790a_0$, and the corresponding Lamb-Dicke parameter is $\eta \approx 0.32$. Since the extra harmonic potential $U_{RL}(r)$ is much weaker than the interatomic interaction in the range of $r < 500a_0$, the distortion of the interatomic potential due to $U_{RL}(r)$ can be neglected. Next we will investigate ultracold collisions of two atoms in a harmonic trap via a self-consistent approach.

C. Self-consistent treatment of the diatomic collision in an optical lattice site

Since the characteristic length scale of the interatomic interaction is typically much smaller than the characteristic length d_h and the s-wave scattering dominates the ultracold collisions under consideration here, the interatomic interaction

$V_{\rm int}(r)$ can be replaced by a zero-range effective-scattering-length pseudopotential [31],

$$V_{\rm eff}(E,\mathbf{r}) = \frac{2\pi\hbar^2}{m} a_{\rm eff}(E)\delta(\mathbf{r})\frac{\partial}{\partial r}r, \tag{53}$$

where E is the total energy of the internal states and relative motion for two atoms in an asymptotic scattering state. The scattering length $a_{\rm eff}(E)$ is written in an energy-dependent form, which can reproduce not only the s-wave phase shifts in the Wigner threshold regime but also the correct asymptotic behavior of the wave function at large r.

We consider the Schrödinger equation of the relative motion by applying the effective pseudopotential,

$$\left(\frac{\mathbf{p}_r^2}{2m} + V_{\rm eff}(E,\mathbf{r}) + H_{\rm hpf}(b)\right)\psi(\mathbf{r}) = E\psi(\mathbf{r}). \tag{54}$$

The eigenvalues can be obtained from solutions of the equation

$$\frac{d_h}{4a_{\rm eff}(E-E_\alpha)} = \frac{\Gamma\left(\frac{3}{4} - \frac{E-E_\alpha}{2\hbar\omega_h}\right)}{\Gamma\left(\frac{1}{4} - \frac{E-E_\alpha}{2\hbar\omega_h}\right)}, \tag{55}$$

which is derived in the same approach in Ref. [32]. Here E_α is the energy of an asymptotic scattering channel $|\alpha\rangle$ of interest. On the other hand, the energy-dependent effective scattering length can be derived from the s-wave phase shift $\delta_0(k)$ for two untrapped atoms scattering in the interatomic potential

$$a_{\rm eff}(E-E_\alpha) = -\frac{\tan\delta_0(k)}{k}, \tag{56}$$

where the incident wave number $k = \sqrt{2m(E-E_\alpha)}/\hbar$. The energy eigenvalue and the effective s-wave scattering length of two atoms scattering in an optical lattice site can be self-consistently solved from Eqs. (55) and (56), which reproduce the asymptotic wave function and the s-wave phase shift.

Figure 7 displays the effective s-wave scattering length $a_{\rm eff}$ (solid curves) as a function of the relative collision energy $\Delta E = E - E_\alpha$ in the entrance channel $|\alpha\rangle = |\Sigma = \frac{9}{2}\rangle$, which is derived from Eq. (55). Here we only consider the positive collision energy $\Delta E \geqslant 0$. For no interatomic interactions, i.e., $a_{\rm eff} = 0$, one recovers the unshifted harmonic oscillator energy $\Delta E = \frac{3}{2}\hbar\omega_h \approx 4.7\ \mu$K of the ground state (the cross in Fig. 7). For infinitely positive and negative scattering lengths $a_{\rm eff} \to \pm\infty$, the ground-state energy is shifted maximally by $\pm\hbar\omega_h$, respectively. In Fig. 7, we also show the energy-dependent s-wave scattering lengths (dashed lines) of two untrapped atoms in different magnetic fields $\mathcal{B}_0$ changing with the relative collision energy ΔE, which are numerically computed via the coupled multichannel-scattering calculation. The intersections (circle) give the self-consistent effective s-wave scattering lengths and energy eigenvalues of two interacting atoms in an optical lattice site. At $\mathcal{B}_0 = 0$, the energy eigenvalue is about $\Delta E \approx 6.1\ \mu$K. When we increase the magnetic field and track the intersection at $\mathcal{B}_0 = 0$, both effective scattering length and energy eigenvalue increase. At the relative collision energy of $\Delta E \approx 8\ \mu$K, the effective scattering length approaches positive infinity and then changes its sign. On the other hand, when $\mathcal{B}_0$ is larger than about 3 gauss, a new intersection comes out on the lower-energy side of the intersection at

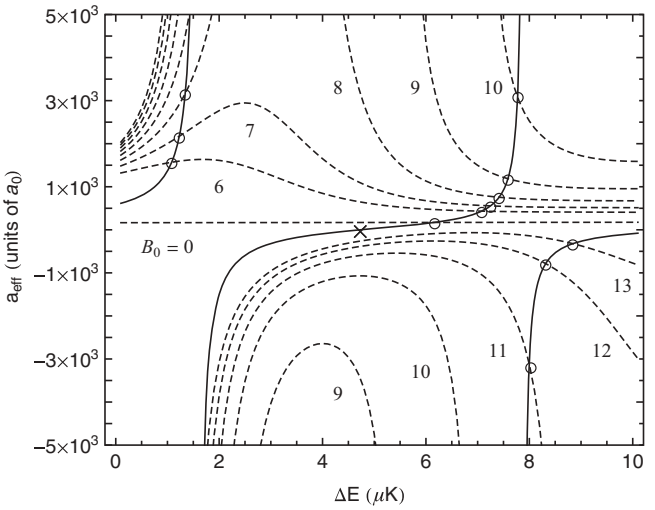

FIG. 7. The s-wave scattering length as a function of the relative collision energy $\Delta E \equiv E - E_\alpha$ of two atoms in the entrance channel $|\Sigma = \frac{9}{2}\rangle$. The solid lines, which are also suitable for two ultracold atoms in the entrance channel $|\Sigma = \frac{11}{2}\rangle$, are derived from Eq. (55). The dashed lines are results from the coupled multichannel-scattering calculation for two untrapped atoms in different magnetic fields $\mathcal{B}_0$. The intersections (circles) give the self-consistent s-wave scattering lengths and energy eigenvalues of two interacting atoms in an optical lattice site. The cross corresponds to the zero effective scattering length $a_{\rm eff} = 0$.

$\mathcal{B}_0 = 0$, which is to say, a new ground state appears instead of the former one. Since the atomic temperature achieved in experiments can be as low as 1 μK, here we only focus on the lower-energy eigenvalues.

Figure 8(a) displays energy eigenvalues of ground states of two interacting atoms in an optical lattice site in entrance channels $|\Sigma = \frac{9}{2}\rangle$ and $|\Sigma = \frac{11}{2}\rangle$ as a function of the external magnetic field. The corresponding effective s-wave scattering lengths changing with $\mathcal{B}_0$ are shown in Fig. 8(b). In the entrance channel $|\Sigma = \frac{11}{2}\rangle$, the new ground state with lower energy appears at magnetic fields $\mathcal{B}_0 > 3.75$ gauss. In both entrance channels $|\Sigma = \frac{9}{2}\rangle$ and $|\Sigma = \frac{11}{2}\rangle$, energy eigenvalues increase with $\mathcal{B}_0$. The corresponding self-consistent scattering lengths approach positive infinity and change signs at about $\mathcal{B}_0 \approx 11.5$ gauss and $\mathcal{B}_0 \approx 14.5$ gauss, respectively. Thus, the interatomic interactions can be turned by the external magnetic field. In the regime of lower-energy eigenvalues, the effective s-wave scattering lengths can be much larger than the characteristic length d_h of the external trapping potential. Since in our model the effective scattering length is chosen to be energy dependent, the self-consistent method still works here, as discussed in Refs. [33–35]. The self-consistent elastic and inelastic scattering rates are shown in Fig. 8(c). In both entrance channels $|\Sigma = \frac{9}{2}\rangle$ and $|\Sigma = \frac{11}{2}\rangle$, increasing $\mathcal{B}_0$ can enlarge elastic scattering rates and suppress the inelastic scattering.

VI. SUMMARY AND DISCUSSION

By applying an approach of tensorial analysis, we have studied the ultracold collisions between metastable bosonic

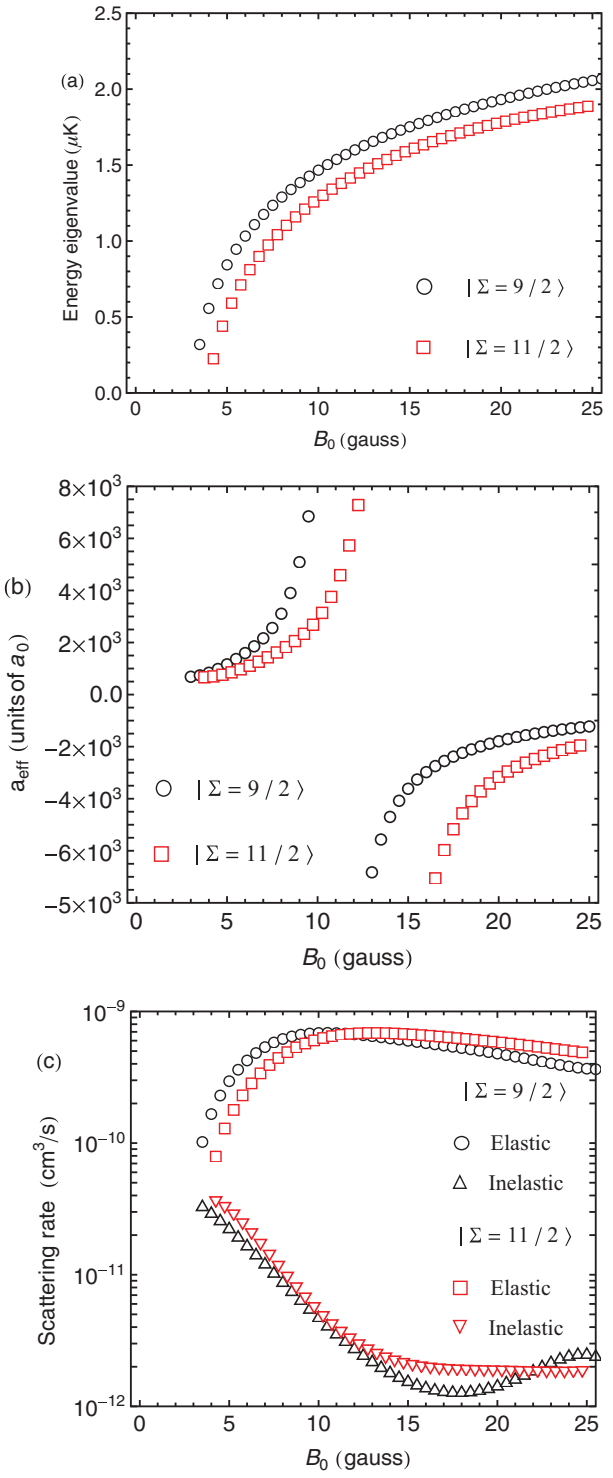

FIG. 8. (Color online) The self-consistent treatment of two interacting atoms in an optical lattice site. (a) The self-consistent energy eigenvalues of two colliding atoms in an optical lattice site relative to energies of the asymptotic scattering channels $|\Sigma = \frac{9}{2}\rangle$ and $|\Sigma = \frac{11}{2}\rangle$, respectively, as a function of magnetic field $\mathcal{B}_0$. $\mathcal{B}_0$ is increased from 0 to 25 gauss with each step of 0.25 gauss. Since the atomic temperature achieved in experiments can be as low as 1 μK, we only show energy eigenvalues in the range from 0 to 2.5 μK. (b) The corresponding self-consistent s-wave scattering lengths as a function of magnetic field $\mathcal{B}_0$. (c) The corresponding elastic and inelastic scattering rates as a function of $\mathcal{B}_0$.

^{88}Sr $[(5s5p)\,^3P_2]$ and fermionic ^{87}Sr $[(5s5p)\,^3P_2$ $(i = \frac{9}{2})]$ atoms at long-range interatomic distances. In the adiabatic approximation, we numerically diagonalized the Hamiltonian matrix including the molecular rotation, interatomic interactions, and the hyperfine interaction of ^{87}Sr, which leads to the complicated adiabatic potential-energy curves. We focused on two fully polarized s-wave entrance channels, in which the adiabatic long-range molecular potential wells exist. As we have pointed out, the scattering physics is governed by the strong anisotropic interatomic interactions, which lead to the pronounced coupling between different scattering channels. Thus, at low temperatures, <10 μK, ultracold collisions of two atoms in the entrance channels of interest are dominated by the inelastic scattering.

We have also studied the dependence of ultracold atomic collisions on the external magnetic field $\mathbf{B}_z = \mathcal{B}_0\mathbf{e}_z$ based on the coupled multichannel-scattering calculation. We find that increasing $\mathcal{B}_0$ not only can enlarge the elastic scattering rates but also can reduce the inelastic scattering of two ultracold atoms in the entrance channels of interest. Moreover, we have investigated the two-body collisions in an optical lattice site. The effective s-wave scattering lengths, energy eigenvalues, and elastic and inelastic scattering rates are self-consistently computed.

As we have said, the effect of short-range interatomic interactions has been neglected in this paper since we do not have the relevant data. However, because (i) the interatomic distances we focused on are far away from the short-range region, for which the interatomic interactions are unable to distort the spin-orbit coupling patterns in ^{88}Sr and ^{87}Sr, and (ii) the repulsive (positive) interaction potential dominates the ultracold collisions of two atoms at the minimal interatomic distance ($r_{\min} = 50a_0$) chosen in this paper, for which no atomic flux penetrates into the inner region, we have confidence in the correctness of the results obtained in this paper.

So far, most research on the ultracold atomic physics, especially the condensed quantum gases in an optical lattice [36], mainly relies on the alkali-metal atoms, which have only one valence electron in their outermost orbits, due to the mature experimental technologies and the thorough understanding of their atomic structures and interatomic interactions [37]. The quantum many-body physics based on alkaline-earth-metal atoms, in particular, the dynamics of phase transitions in an optical lattice, has not been well developed because of less relevant knowledge of the interatomic interactions. However, an ensemble of ultracold atoms with two valence electrons must lead to new phenomena, which are different from those based on the alkali-metal atoms, such as a novel degenerate Fermi mixture with an SU(2) $\times$ SU(6) symmetry [38]. For this reason, our research in this paper is meaningful. In the future, we would like to extend our study to the quantum many-body physics of a mixture of bosonic and spin-polarized fermionic (^{88}Sr-^{87}Sr) atoms in optical lattices.

ACKNOWLEDGMENT

The author would like to thank Hidetoshi Katori for useful discussions and suggestions.

[1] F. Riehle, H. Schnatz, G. Zinner, K. Zeiske, B. Lipphardt, and J. Helmcke, Laser Physics **6**, 237 (1996).
[2] M. Takamoto, F.-L. Hong, R. Higashi, and H. Katori, Nature (London) **435**, 321 (2005).
[3] M. Takamoto, T. Takano, and H. Katori, Nat. Photonics **5**, 288 (2011).
[4] D. Yu, Phys. Rev. A **85**, 032705 (2012).
[5] A. J. Daley, M. M. Boyd, J. Ye, and P. Zoller, Phys. Rev. Lett. **101**, 170504 (2008).
[6] M. Antezza and Y. Castin, Phys. Rev. Lett. **103**, 123903 (2009).
[7] D. Yu, Phys. Rev. A **84**, 043833 (2011).
[8] H. Katori, T. Ido, Y. Isoya, and M. Kuwata-Gonokami, Phys. Rev. Lett. **82**, 1116 (1999).
[9] T. Binnewies, G. Wilpers, U. Sterr, F. Riehle, J. Helmcke, T. E. Mehlstäubler, E. M. Rasel, and W. Ertmer, Phys. Rev. Lett. **87**, 123002 (2001).
[10] Y. N. Martinez de Escobar, P. G. Mickelson, M. Yan, B. J. DeSalvo, S. B. Nagel, and T. C. Killian, Phys. Rev. Lett. **103**, 200402 (2009).
[11] S. Stellmer, M. K. Tey, B. Huang, R. Grimm, and F. Schreck, Phys. Rev. Lett. **103**, 200401 (2009).
[12] S. Stellmer, M. K. Tey, R. Grimm, and F. Schreck, Phys. Rev. A **82**, 041602(R) (2010).
[13] S. Kraft, F. Vogt, O. Appel, F. Riehle, and U. Sterr, Phys. Rev. Lett. **103**, 130401 (2009).
[14] M. Yasuda and H. Katori, Phys. Rev. Lett. **92**, 153004 (2004).
[15] S. B. Nagel, C. E. Simien, S. Laha, P. Gupta, V. S. Ashoka, and T. C. Killian, Phys. Rev. A **67**, 011401(R) (2003).
[16] A. Derevianko, S. G. Porsev, S. Kotochigova, E. Tiesinga, and P. S. Julienne, Phys. Rev. Lett. **90**, 063002 (2003).
[17] R. Santra and C. H. Greene, Phys. Rev. A **67**, 062713 (2003).
[18] V. Kokoouline, R. Santra, and C. H. Greene, Phys. Rev. Lett. **90**, 253201 (2003).
[19] P. Feng, D. Hoffmann, and T. Walker, Phys. Rev. A **47**, R3495 (1993).
[20] A. R. Gorges, N. S. Bingham, M. K. DeAngelo, M. S. Hamilton, and J. L. Roberts, Phys. Rev. A **78**, 033420 (2008).
[21] T. H. M. Van den Berg and A. van der Avoird, Chem. Phys. Lett. **160**, 223 (1989).
[22] L. Olschewski, Z. Phys. **249**, 205 (1972).
[23] O. Häusser, T. Faestermann, I. S. Towner, T. K. Alexander, H. R. Andrews, J. R. Beene, D. Horn, D. Ward, and C. Broude, Hyperfine Interact. **4**, 196 (1978).
[24] A. Derevianko, Phys. Rev. Lett. **87**, 023002 (2001).
[25] S. M. Heider and G. O. Brink, Phys. Rev. A **16**, 1371 (1977).
[26] B. R. Johnson, J. Comput. Phys. **13**, 445 (1973).
[27] J. L. Bohn and P. S. Julienne, Phys. Rev. A **56**, 1486 (1997).
[28] J. M. Hutson, New J. Phys. **9**, 152 (2007).
[29] P. Rosenbusch, S. Ghezali, V. A. Dzuba, V. V. Flambaum, K. Beloy, and A. Derevianko, Phys. Rev. A **79**, 013404 (2009).
[30] X. Zhou, X. Xu, X. Chen, and J. Chen, Phys. Rev. A **81**, 012115 (2010).
[31] R. Stock, I. H. Deutsch, and E. L. Bolda, Phys. Rev. Lett. **91**, 183201 (2003).
[32] T. Busch, B.-G. Englert, K. Rzazewski, and M. Wilkens, Found. Phys. **28**, 549 (1998).
[33] E. L. Bolda, E. Tiesinga, and P. S. Julienne, Phys. Rev. A **66**, 013403 (2002).
[34] D. Blume and C. H. Greene, Phys. Rev. A **65**, 043613 (2002).
[35] G. Peach, I. B. Whittingham, and T. J. Beams, Phys. Rev. A **70**, 032713 (2004).
[36] M. Greiner, O. Mandel, T. Esslinger, T. W. Hänsch, and I. Bloch, Nature (London) **415**, 39 (2002).
[37] E. R. I. Abraham, W. I. McAlexander, C. A. Sackett, and R. G. Hulet, Phys. Rev. Lett. **74**, 1315 (1995).
[38] S. Taie, Y. Takasu, S. Sugawa, R. Yamazaki, T. Tsujimoto, R. Murakami, and Y. Takahashi, Phys. Rev. Lett. **105**, 190401 (2010).